Published in final edited form as:

IEEE Trans Ultrason Ferroelectr Freq Control. 2017 March ; 64(3): 537–543. doi:10.1109/TUFFC.2016.2638801.

Continuous subresolution displacements in finite difference simulations of ultrasound propagation and imaging

Gianmarco Pinton[1]

[1]Department of Biomedical Engineering, University of North Carolina at Chapel Hill and North Carolina State University

Abstract

Time domain finite difference simulations are used extensively to simulate wave propagation. They approximate the wave field on a discrete domain with a grid spacing that is typically on the order of a tenth of a wavelength. The smallest displacements that can be modeled by this type of simulation are thus limited to discrete values that are integer multiples of the grid spacing. This paper presents a method to represent continuous and subresolution displacements by varying the impedance of individual elements in a multi-element scatterer. It is demonstrated that this method removes the limitations imposed by the discrete grid spacing by generating a continuum of displacements as measured by the backscattered signal. The method is first validated on an ideal perfect correlation case with a single scatterer. It is subsequently applied to a more complex case with a field of scatterers that model an acoustic radiation force induced displacement used in ultrasound elasticity imaging. A custom finite difference simulation tool is used to simulate propagation from ultrasound imaging pulses in the scatterer field. These simulated transmit-receive events are then beamformed into images which are tracked with a correlation based algorithm to determine the displacement. A linear predictive model is developed to analytically describe the relationship between element impedance and backscattered phase shift. The error between model and simulation is $\lambda/1364$, where λ is the acoustical wavelength. An iterative method is also presented that reduces the simulation error to $\lambda/5556$ over one iteration. The proposed technique therefore offers a computationally efficient method to model continuous subresolution displacements of a scattering medium in ultrasound imaging. This method has applications that include ultrasound elastography, blood flow, and motion tracking. This method also extends generally to finite difference simulations of wave propagation, such as electromagnetic or seismic waves.

I. Introduction

Finite difference simulations can solve the full acoustical wave equation without introducing approximations to the propagation physics [1], [2], [3]. The advantage of finite differences simulations of ultrasound imaging is that they can model fine heterogeneities, phase aberration, multiple scattering, and the generally complex acoustical anatomy of the human body [3], [4]. The disadvantage of finite difference modeling of the full-wave equation is its

Further author information: Send correspondence to G. Pinton: gfp@unc.edu.

computational cost which is significantly higher than ultrasound imaging simulations that solve approximations to the wave equation or that convolve the imaging impulse response with a field of scatterers [5].

When modeling small displacements with finite differences the computational cost can become even more restrictive. Finite difference methods subdivide a grid into a rectangular mesh so the mesh size imposes a discrete limit on scatterer movement, i.e. a scatterer cannot appear in between mesh points. This is unlike many finite element simulations which can use an unstructured and adaptive grid [6]. Therefore, for a direct representation of displacement, the smallest unit of displacement is determined by the spatial grid size. Typical displacements in ultrasound elastography are on the order of microns [7], [8]. For example, to model a 1 micron displacement directly in 2D for a 3×7 cm field of view and a 2MHz emission would require 2.1×10^9 grid points. This is an unnecessarily refined grid and unnecessarily large computation because a grid spacing of $\lambda/15$, or 51 μm, would be sufficient to model an ultrasound pulse with a 100 dB dynamic range [4]. For this coarser grid spacing the number of points in the simulation is 8.0×10^5, which is almost four orders of magnitude smaller. Thus a displacement method that can be implemented on a coarse grid would provide significant computational benefits.

The objective of this paper is therefore to present and validate a method that can generate continuous subresolution displacements with a coarse finite difference grid spacing. The proposed method is based on the notion that a single scatterer can be composed of multiple elements. The total impedance of the scatterer is conserved but it can “flow” in between individual elements of the scatterer. The phase of the backscattered wave is shifted by changing the impedance distribution within the scatterer therefore generating an observed displacement. The process can happen continuously by changing the *values* of the scatterer elements rather than the *position* of the scatterer. This method is referred to as impedance flow for the remainder of the paper.

In the first part of the paper the impedance flow method is described with equations relating the impedance value of individual elements within a single scatterer to the observed displacement. This model is then verified with an idealized case of a single scatterer. The Fullwave finite difference simulation tool [3] is used to propagate a wave to a single impedance flow scatterer and the backscatterered signal is used to determine the displacement. The error between the model and the simulated impedance flow scatterer is characterized as a continuous subresolution function of displacement.

Once the impedance flow method has been established for a single scatterer a more complex ultrasound elastography scenario is investigated. A 2D field of scatterers is used as an input to the Fullwave simulation to generate ultrasound images with fully developed speckle. These scatterers are then displaced *in silico* with an acoustic radiation force impulse. This provides a continuous 2D distribution of displacements which is used to displace the scatterers and subsequently to simulate displaced ultrasound images. The proposed impedance flow scatterers are compared to a discrete implementation of scatterer motion. It is shown that the proposed method can accurately model this continuous and complex

scatterer motion at a computational cost that is many orders of magnitude less than an equivalent simulation with discretely displaced scatterers.

II. Analytical representation of the impedance flow method

Fig. 1 illustrates that for a direct representation of scatterer movement on a finite difference grid the smallest unit of displacement is determined by the spatial grid size. The image on the left is shows a reference scatterer on a 5 × 6 grid point mesh. The image in the middle illustrates the scatterer displaced down by a single mesh point, which is the smallest possible discrete unit of displacement. The proposed impedance flow method is shown on the right. This scatterer is composed of two elements and the impedance "flows," in a conservative sense, from one element to the other. The backscattered ultrasound originates in part from the first element, and in part from the second. By adjusting the impedance the amount of backscattered energy can be weighted preferentially from the first or second element. The hypothesis is that for two elements that are much smaller than the wavelength that they will act, physically and numerically, as a single scatterer that can produce a continuous subresolution phase shift in the backscattered wave.

The impedance values of the two elements in the scatterer can vary arbitrarily. These two degrees of freedom can be constrained by 1) the desired magnitude of the backscattered wave and 2) the phase of the backscattered wave. Let z_m be the medium impedance, z_1 and z_2 the impedance of the first and second elements in the scatterer. The magnitude of the backscattered wave is proportional to the observed impedance mismatch between the scatterer and the background medium. Here we denote the observed scatterer impedance as z_0. We assume that the wave is sufficiently large compared to the scatterer so that the observed impedance is given simply by the average of the two elements:

$$z_0 = \frac{z_1 + z_2}{2} \quad (1)$$

Physically, the observed scatterer impedance is a fixed quantity that is invariant under displacement. However the elements z_1 and z_2 can vary individually. Here they are allowed to vary until they reach the same value as the background, z_m because when the scatterer element has the same impedance value as the background it stops scattering. This second constraint can thus be written as

$$z_1, z_2 \leq z_m \quad (2)$$

In this equation we assume that $z_0 < z_m$ although an equivalent relationship with an inverted inequality and with $z_0 > z_m$ would be equally valid.

The two limit cases are easily understood. If $z_2 = z_m$ then the second element is transparent and the scatterer is in the configuration shown on the left of Fig. 1. Similarly when $z_1 = z_m$ the scatterer is in the configuration shown in the middle plot of Fig. 1. Therefore, according

to this model, the left and middle plots of Fig. 1 are interpreted to have a scatterer composed of two elements, even though the scatterer appears to have only one element. For intermediate values of γ, shown on the right of Fig. 1, the impedance can be expressed by two parametric equations for z_1 and z_2

$$z_1=(1-\gamma)(2z_0-z_m)+\gamma z_m \quad (3)$$

$$z_2=\gamma(2z_0-z_m)+(1-\gamma)z_m \quad (4)$$

where the fractional shift parameter γ has values $0 \leq \gamma \leq 1$. Note that Eqs. 3 and 4 satisfy Eq. 1 for all values of γ. For the midpoint value of $\gamma = 1/2$ the impedance of the elements is $z_1 = z_2 = z_0$, the average impedance of the scatterer. According to Eqs. 3 and 4 the shaded elements in the left and middle plots in Fig. 1 have an impedance of $2z_0 - z_m$ and the non-shaded elements have an impedance of z_m. Then, according to the two-element interpretation, the impedance for the scatterer is given by $(2z_0 - z_m + z_m)/2 = z_0$, which confirms that the total impedance for the two-element scatterer is consistent with the definition. In the following section we test the hypothesis that the phase of the backscattered signal varies linearly as a function of the impedance parameter, γ.

III. Model validation and calibration with Fullwave FDTD acoustic simulations

The validity of the proposed impedance flow method was tested with Fullwave, a custom finite difference time domain (FDTD) simulation tool that has been used extensively in the context of ultrasound imaging [3], [4]. The simulation domain was chosen to be a 2.4 cm wide by 7 cm deep with a grid spacing, Δx, of 15 points per wavelength with respect to a 2 MHz transmit frequency. This is equivalent to a 468 × 1364 point domain, with a grid spacing of $51\mu m$. A linear array with an F/2 unapodized aperture was used to focus a 2 cycle pulse at a depth of 45mm.

The Courant-Friedrichs-Lewy (CFL) condition, which determines the stability and convergence of the finite difference code [9], is defined as

$$\mathrm{CFL}=\frac{c\Delta t}{\Delta x} \quad (5)$$

where c is the speed of sound and Δt is the size of the time step. The CFL condition fixes the ratio of the time step to the grid spacing and here it was set to 0.4. For the discrete displacement shown in Fig. 1 the backscattered signal is delayed by $2\Delta x$. According to Eq. 5 this is equivalent to a time delay of $5\Delta t$. In subsequent discussion displacement by a spatial element and displacement by five time samples will be used interchangeably. Table I summarizes the these equivalence relationships between space, time, and grid sizes. A speed

of sound c_0 = 1540 m/s was assumed. There is a factor of 2 between displacement and time delay due to the range equation, where the distance d depends on the total travel time t according to $t = 2d/c_0$.

A set of simulations was performed with a single subresolution scatterer at the focus with a mean impedance set to $z_0 = 0.9875 z_m$. The density ρ was set to a constant 1000 kg/m^3 for the medium and scatterers so that only the speed of sound was used to determine the impedance. The speed of sound of the background medium was set to 1540 m/s and the speed of sound for the two elements in the scatterer was allowed to vary according to Eqs. 3 and 4. Thus, according to the impedance relationship $z = \rho c$, the speed variations have a maximum of 1540 m/s and a minimum of 1502 m/s.

To determine the displacement the backscattered echo from the original scatterer was compared to the echo from the displaced scatterer. This was performed with a correlation based displacement tracking code [10] which has been validated in the context of acoustic radiation force impulse based imaging and is currently used extensively in ultrasound elastography. The raw radio-frequency (RF) data was interpolated by a factor of three with a cubic spline algorithm. Normalized cross correlation with a kernel length of 3λ (2.3 mm) was then used to determine the discrete correlation function over a search range of $2/3\lambda$ (i.e. 10 time samples, at the original sampling rate). Finally a continuous estimate of the displacement and correlation value was obtained with a continuous parabolic fit of the peak of the correlation function. This peak corresponds to the axial displacement at a single location.

Fig. 2 shows the displacement as a function of the impedance parameter, γ. It compares the displacement measured in the simulation (dashed line) with the linear prediction described in the previous section (solid line). There is little visible difference between these two lines. The error is shown on the right of Fig. 2. The root-mean-square (RMS) error is 10.99×10^{-3} spatial samples, or in terms of the acoustical wavelength, $\lambda/1364$. Even though the error is much smaller than the wavelength, the impedance flow method can be improved further.

A. Improvement of the simulated displacement accuracy with grid-dependent calibration

The data in Fig. 2 was used as calibration curve so that the simulated displacements would match the linear prediction more closely. This was implemented by simply using the dashed curve of Fig. 2 as a lookup table for the desired displacement in the Fullwave simulation. The results of this calibrated simulation are shown in Fig. 3, for which the RMS error is 2.699×10^{-3} spatial samples, or equivalently $\lambda/5556$. This is approximately a factor of four improvement compared to the uncalibrated measurements in Fig. 2.

To achieve even higher accuracy this calibration procedure can be repeated in an iterative fashion. For the grid size considered here performing over two iterations yielded diminishing returns in terms of accuracy, suggesting that at these low errors the limiting factor may be the machine precision of computer arithmetic. In summary, depending on the desired accuracy, the element impedance can be determined directly from the linear prediction or, for added precision, with a calibration simulation. Compared to the analytical model the disadvantage of the calibration approach is that a new simulation must be performed if the

grid parameters are changed. However if a calibration curve has been determined for a specific grid spacing then any grid with that same spacing and any scatterer on that grid can use that single calibration curve.

IV. Validation of the impedance flow method for radiation force displacements

A radiation force based displacement, such as those used in ultrasound elastography [7], [8] was determined based on the approximation that the displacement is proportional to the intensity. In reality the displacement is more complex and is given by the time-dependent interaction of the radiation force, which is only approximately proportional to the intensity, with the soft tissue viscoelastic response [11]. These effects are ignored as they are outside the scope of this paper.

The intensity distribution of an F/8 transducer with a 45 mm focus was calculated with the Fullwave simulation. The remainder of the transducer and simulation parameters remained unchanged with respect to the description in the previous section. The displacement was assumed to be directly proportional to the radiation force and it is shown on the left of Fig. 4 in units of time samples. In terms of physical displacement this corresponds to a maximum range of 77 μm. This is a relatively large displacement compared to the typical ranges induced by acoustic radiation force, and it is meant to favor the discrete element representation of displacement, which can't model small displacements, over the proposed impedance flow method which is designed to model small displacements.

A field of subresolution scatterers, shown in the middle plot of Fig. 4, was used to simulate a uniformly scattering medium. Over 12 scatterers per resolution volume were used so that the speckle statistics were fully developed [12]. These scatterers were then displaced either discretely or according the impedance flow method. For the discrete element representation of displacement the theoretical scatterer position was rounded to its nearest grid position in space. Since movement by a single element is equivalent to a 51μm displacement this operation rounded all displacements to either 0μm or 51μm.

At the scale illustrated in Fig. 4 there is no visual difference between the three scatterer fields (reference, discretely displaced, and the impedance flow method). To illustrate the difference between the simulation fields Fig 5 zooms in on the focal region at a depth between 43 and 46 mm. Each of the individual scatterer elements on the right plot of Fig. 5 continuously represents the displacement in the manner illustrated on the right of Fig. 1. The proposed impedance flow method was used to represent a maximum shift of half a pixel in the positive or half a pixel in the negative direction. A shift of 0.75 pixels in the positive direction, for example, would result in a discrete shift of positive one pixels and a negative impedance flow shift of 0.25 pixels. For these simulations the simpler linear prediction impedance flow method shown in Fig. 2 was chosen rather than the more accurate calibrated impedance flow method. Results shown in subsequent sections demonstrate that this simpler model is sufficient because its error is smaller than the error associated with fundamental tracking limits [13].

A. Generation of ultrasound images with impedance flow scatterers

The Fullwave tool was used to generate ultrasound images based on simulations of the propagation physics. This technique has been described previously [3] and it is summarized briefly here. Since the simulation tool is based on propagation physics the process to generate an B-mode image is the same as what is typically performed with an ultrasound scanner. A focused transmit beam is sent into the medium. The scatterers reflect sound back towards the surface. The simulated array is used to “receive” the basckscattered wave and conventional delay-and-sum beamforming is used to generate a B-mode image.

The resulting B-mode image is shown on the right of Fig. 4 for the reference scatterer field. At this scale the discretely displaced scatterers and scatterers displaced according to the proposed impedance flow method appear to be identical and therefore have not been plotted. These images show that the first order scattering behavior of the impedance flow scatterers is equivalent to scattering from conventional uniform scatterers. The scatterer displacements are small enough that there is no discernible difference between the B-mode images corresponding to the three scatterer fields (reference, discretely displaced, and the impedance flow method). However there are measurable differences in the RF data which can be measured with tracking algorithms.

B. Displacement estimation

The beamformed RF data along the centerlines of the three B-mode images corresponding to the scatterer fields in Fig. 5 is shown in Fig. 6. The depth is zoomed in to a 5 mm region at the focus, between 42.5mm and 47.5mm. There is a clear phase shift between the reference (solid cyan), the discretely displaced scatters (dashed red) and the impedance flow method (dash-dotted black).

To quantify the displacements the previously described correlation based tracking algorithm [10] was applied to the beamformed RF data generated by the simulations. The parameters used for this tracking algorithm remained the same as those described in Section III.

To remove variability associated with individual speckle realizations the displacements were calculated for 20 independent scatterer realizations. Each independent realization was used to construct three fields: 1) the reference scatterers, 2) discretely displaced scatterers, and 3) impedance flow scatterers.

The average displacements estimated for the 2D scatterer fields are shown on the left of Fig. 7 for the discretely displaced scatterers, and on the right of Fig. 7 for the impedance flow scatterers. Note that these calculated displacements can be compared to the analytical displacement shown on the left of Fig. 4. As expected the discretely displaced scatterers yielded a uniform displacement estimate rounded to the nearest unit of the spatial grid, which is equivalent to a 5 time sample displacement. For this grid spacing the discretely displaced scatterer field yields a binary approximation to the analytical field. The displacements for the impedance flow scatterers, on the other hand, closely resemble the analytical displacements.

Fig. 8 directly compares the analytical displacement (solid cyan) to the discretely displaced scatters (dashed red) and the impedance flow scatterers (dash-dotted black) along the center axis of propagation (left), and laterally at the focus (right). The error bars were calculated based on the standard deviation from the different scatterer realizations.

These plots show clearly that scatterers that were discretely displaced yielded a uniform displacement estimate rounded to the nearest unit of the spatial grid, i.e. a 0 or 5 time sample displacement. There is a small boundary region of as the displacement estimates transition from one quantum of displacement to another, which is consistent with the spatial resolution of the imaging system.

The impedance flow scatterers generate a continuum of displacements that closely match the analytical displacements. The RMS error between the analytical and the impedance flow calculation is 0.024 spatial samples or equivalently $\lambda/614$. This is larger than the displacement error for a single scatterer as calculated in Section III which was 0.011 spatial samples.

In addition to the calibration error described in Section III, there are two other main sources of error. The first is due to the individual speckle realization. Since the scatterers have moved the displaced backscattered signal does not perfectly match the reference backscattered signal. This generates correlation values that are on average 0.9914 and which places a fundamental limit on the accuracy of the displacement estimates imposed by the Cramer-Rao lower bound [13], [10]. This decorrelation is principally responsible for the observed variability in the error bars, which on average is 0.020 spatial samples. The second error mechanism is due to the size of the correlation kernel, which is 3λ or equivalently 45 spatial samples. Motion that is smaller than the kernel size tends to be blurred out. In Fig. 8 this blurring is apparent in the peak at 26 mm depth and the trough at 30 mm depth. This is also why the main peak at 45mm depth slightly underestimates the true displacement and the sides slightly overestimate the true displacement.

Therefore there is more error due to jitter imposed by the fundamental tracking limits and blurring from the finite kernel length than error from the impedance flow scattering. The proposed method can accurately represent a continuum of displacements and is thus able to capture the relevant scattering physics associated with small continuous displacements.

V. Equivalent computational cost for discrete displacements

As was mentioned in the introduction, the displacement resolution of the discretely displaced scatterers can be increased by simply constructing a simulation with finer grid spacing. However the computation time for a 2D finite difference simulation increases cubically as a function of the inverse of the grid spacing and the memory requirements increase quadratically.

The error quantification from Section III can be used to determine the equivalent grid size that would be required to obtain the same precision as the impedance flow displacement with a discrete displacement. The simulations presented here had a run time of approximately 20 minutes on a single core of an Intel Xeon E5-2650 v2 2.60GHz CPU. To

obtain a displacement resolution equivalent to 0.011 spatial samples a grid that is finer by a factor of 90.9 would be required. The computation time would increase by 7.5×10^5 and the memory requirement would increase by 8.3×10^3.

For the calibrated impedance flow simulation with one iteration the grid would have to be refined by a factor of 370. This would increase the computation time by a factor of 5.1×10^7 and the memory requirements by 1.4×10^5.

For a 3D simulation the increase in computation time is quartic and the increase in memory is cubic. The computational costs would therefore increase even more dramatically than in the 2D case.

VI. Discussion and Conclusion

The strength of finite difference methods is that they can be used to model the full wave propagation physics in heterogeneous materials. Since the focus of this paper was on validation of the method, simple configurations, either a single scatterer or a uniformly distributed field of scatterers, were used. In fact, for these configurations other simulation methods, could be used to calculate the backscattererd acoustics with less computational effort.

The applications of the impedance flow scatterers and finite differences in general is therefore best suited to more complex fields. For example the Fullwave code has been used to model harmonic imaging [3], reverberation clutter [4], and spatial coherence imaging [14] with detailed anatomical models of the human body and the impedance flow method opens up the possibility of modeling of displacements within these more complex domains. Another application is to the development of more accurate tracking algorithms, such as those used to track shear shock waves which is a challenging tracking problem due to the discontinuities in the particle velocity [15].

Ultrasonic displacement tracking is more accurate along the depth axis [16] and here only displacements along the depth axis were considered. However the impedance flow method can be extended to model 2D and 3D subresolution displacements. This entails generating scatterers with at least a 2×2 element configuration for 2D displacements and a 2×2×2 element configuration for 3D displacements. The mechanism for generating displacements remains the same, i.e. the total impedance of the scatterer is conserved, and the impedance "flows" in between the constitutive elements of the scatterer. This flow can be applied independently along different axes. For example, for a for a 2×2 scatterer a fractional shift γ can be applied along the propagation axis, then a second shift η across it.

The examples presented and the development provided consider isolated scatterers in a uniform background, so that the surrounding grid points have a uniform impedance z_m. The method could be extended to the case of generally random impedance values throughout the grid provided that the scatterers are defined by two grid elements. Then the proposed impedance flow method can be applied directly to each element pair.

In summary, the impedance flow scattering method of representing subresolution displacements was developed and described theoretically. Finite difference simulations were shown to closely follow theoretical predictions and the error between model and simulation was $\lambda/1364$. This error can be reduced iteratively by calibrating the simulation, in which case the agreement with theory was reduced to $\lambda/5556$ over one iteration. It was shown that the impedance flow method can accurately represent the displacements induced by acoustic radiation force, which has particular applications to ultrasound elastography. In general this method has applications to areas of ultrasound where displacement tracking is used, such as blood flow or motion tracking. Finite difference simulations are used widely to model wave propagation and the impedance flow method would be simple to implement in other domains such as seismology or electromagnetism.

Acknowledgments

The authors would like to acknowledge support from the NIH R01 NS091195-01.

References

1. Mast TD, Hinkelman LM, Orr MJ, Sparrow VW, Waag RC. Simulation of ultrasonic pulse propagation through the abdominal wall. Journal of the Acoustical Society of America. Aug; 1997 102(2):1177–1190. [PubMed: 9265762]
2. Mast TD. Two- and three-dimensional simulations of ultrasonic propagation through human breast tissue. Acoustics Research Letters Online. 2002; 3(2):53–58.
3. Pinton G, Dahl J, Rosenzweig S, Trahey G. A heterogeneous nonlinear attenuating full-wave model of ultrasound. Ultrasonics, Ferroelectrics and Frequency Control, IEEE Transactions on. 2009; 56(3):474–488.
4. Pinton GF, Trahey GE, Dahl JJ. Erratum: Sources of image degradation in fundamental and harmonic ultrasound imaging: a nonlinear, full-wave, simulation study [apr 11 754–765]. Ultrasonics, Ferroelectrics and Frequency Control, IEEE Transactions on. 2011; 58(6):1272–1283.
5. Jensen JA, Svendsen NB. Calculation of pressure fields from arbitrarily shaped, apodized, and excited ultrasound transducers. IEEE Trans Ultrason, Ferroelec, Freq Contr. 1992; 39(2):262–267.
6. Babuvška I, Rheinboldt WC. Error estimates for adaptive finite element computations. SIAM Journal on Numerical Analysis. 1978; 15(4):736–754.
7. Nightingale K, Soo MS, Nightingale R, Trahey G. Acoustic radiation force impulse imaging: in vivo demonstration of clinical feasibility. Ultrasound in medicine & biology. 2002; 28(2):227–235. [PubMed: 11937286]
8. Bercoff J, Tanter M, Fink M. Supersonic shear imaging: a new technique for soft tissue elasticity mapping. Ultrasonics, Ferroelectrics and Frequency Control, IEEE Transactions on. 2004; 51(4): 396–409.
9. Trangenstein, J. Numerical Solution of Hyperbolic Partial Differential Equations. Cambridge University Press; 2009.
10. Pinton G, Dahl J, Trahey G. Rapid tracking of small displacements with ultrasound. Ultrasonics, Ferroelectrics and Frequency Control, IEEE Transactions on. 2006; 53(6):1103–1117.
11. Palmeri ML, Sharma AC, Bouchard RR, Nightingale RW, Nightingale RW. A finite-element method model of soft tissue response to impulsive acoustic radiation force. Ultrasonics, Ferroelectrics, and Frequency Control, IEEE Transactions on. 2005; 52(10):1699–1712.
12. Wagner RF, Smith SW, Sandrik JM, Lopez H. Statistics of speckle in ultrasound b-scans. Sonics and Ultrasonics, IEEE Transactions on. 1983; 30(3):156–163.
13. Walker WF, Trahey GE. A fundamental limit on delay estimation using partially correlated speckle signals. IEEE Trans Ultrason, Ferroelect, Freq Contr. Mar; 1995 42(2):301–308.

14. Pinton G, Trahey G, Dahl J. Spatial coherence in human tissue: implications for imaging and measurement. Ultrasonics, Ferroelectrics, and Frequency Control, IEEE Transactions on. 2014; 61(12):1976–1987.
15. Pinton G, Gennisson J-L, Tanter M, Coulouvrat F. Adaptive motion estimation of shear shock waves in soft solids and tissue with ultrasound. Ultrasonics, Ferroelectrics, and Frequency Control, IEEE Transactions on. 2014; 61(9):1489–1503.
16. Jensen, JA. Estimation of blood velocities using ultrasound: a signal processing approach. Cambridge University Press; 1996.

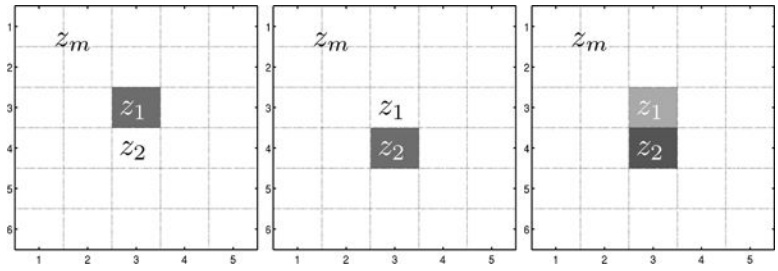

Fig. 1.

Illustration of a 5 × 6 point grid. Left: a reference scatterer. Middle: a scatterer with a discretized displacement of one element. Right: a subresolution displacement based on the proposed impedance flow scattering.

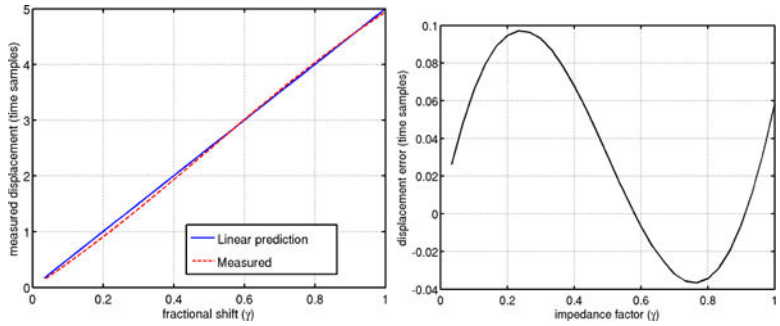

Fig. 2.

The left plot shows the displacement as a function of the impedance parameter γ according to theoretical prediction (solid line) and measured with the Fullwave FDTD simulation (dashed). The right plot shows the error between theory and measurement.

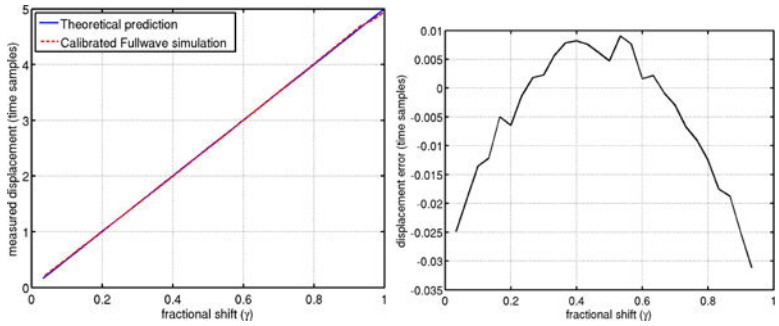

Fig. 3.

The left plot shows the displacement as a function of the impedance parameter γ according to the theoretical prediction (solid line) and measured with the calibrated Fullwave FDTD simulation (dashed). With a single correction iteration the RMS error is a reduced by a factor of 4 compared to Fig. 2. The right plot shows the error between theory and measurement.

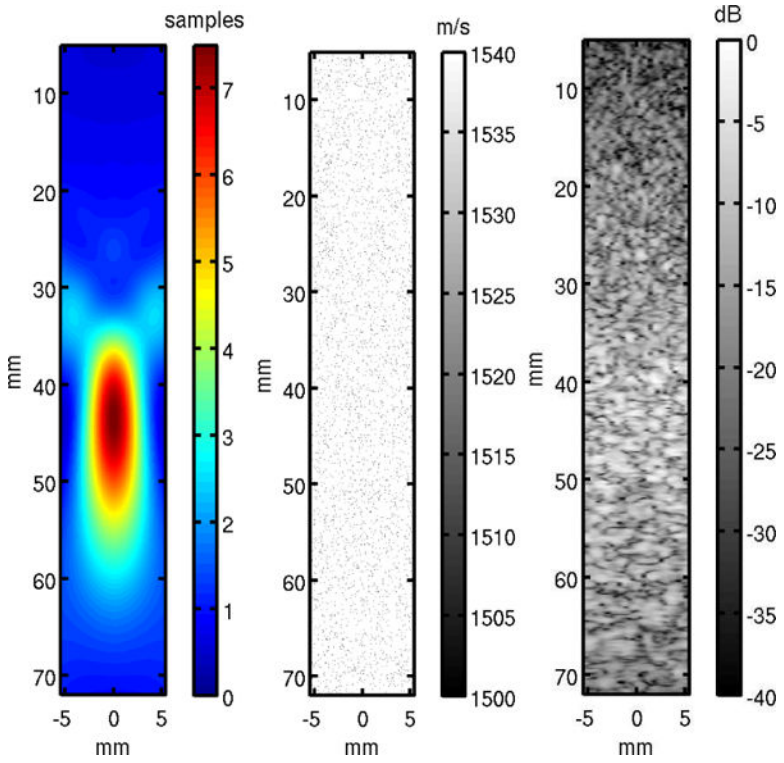

Fig. 4.

The acoustic radiation force from a focused transducer was used to directly approximate the displacements in time samples (left). The reference field of subresolution scatterers is shown in the middle and the corresponding B-mode image based on the transmit-receive Fullwave simulations is shown on the right.

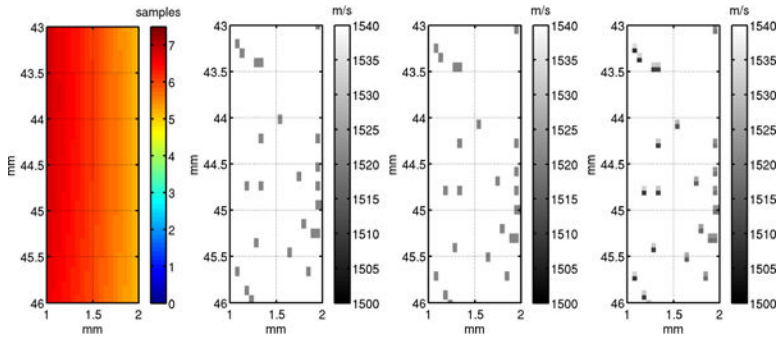

Fig. 5.

A zoomed-in version of Fig. 4. The acoustic radiation force is shown on the left. The reference field of subresolution scatterers (middle left) was displaced discretely on spatial grid points (middle right) or according to the proposed impedance flow method (right).

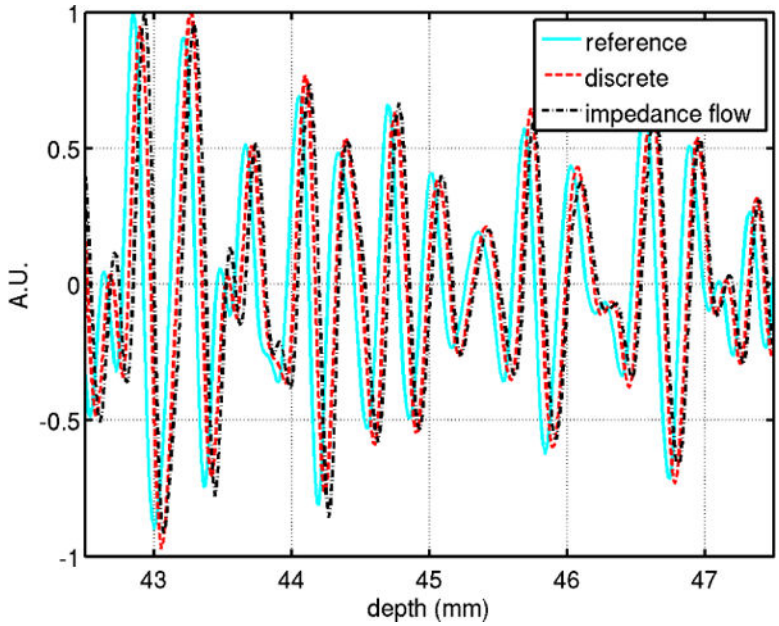

Fig. 6.

The beamformed RF data on the centerline of the three scatterer fields shown in Fig. 5 zoomed in to the focal region between 42.5mm and 47.5mm. The amplitude of the RF data is represented in arbitrary units (A.U.).

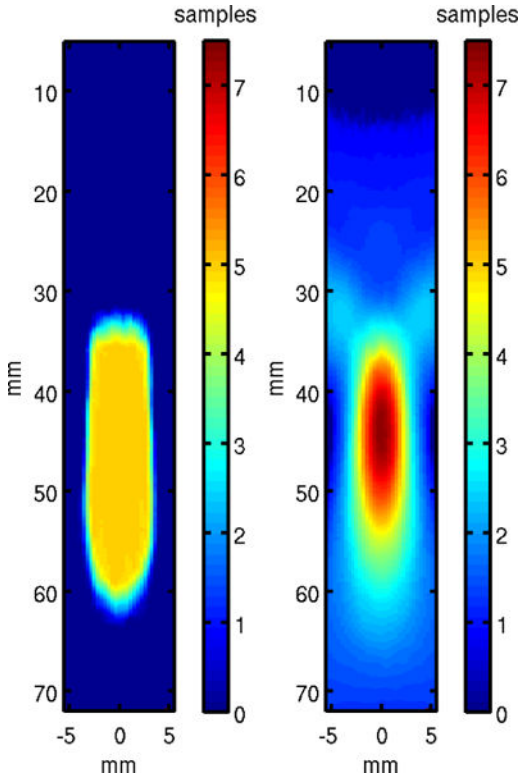

Fig. 7.

The displacements calculated from the backscattered RF data using a correlation based algorithm for the discretely displaced scatterers (left), and the impedance flow scatterers (right). Cf with the analytical displacements shown on the left of Fig. 4.

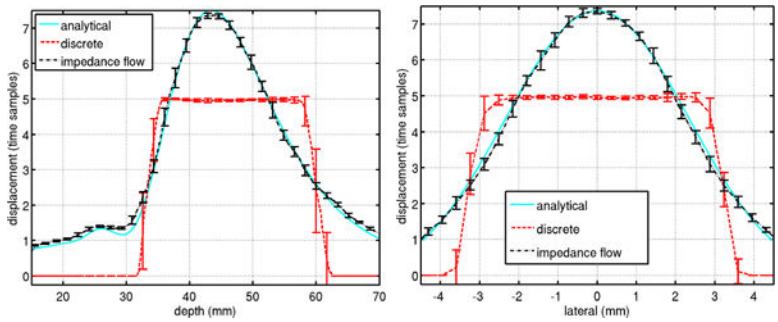

Fig. 8.

A comparison of the analytical displacement (solid cyan) to the displacements calculated with the discretely displaced scatters (dashed red) and impedance flow scatterers (dash-dotted black) along the center axis of propagation (left), and laterally at the focus (right).

TABLE I

Displacement equivalence

Spatial samples	Displacement	Time samples	Time delay
1	51μm	5	67 ns